Project: **1233**

Project title: **MOD: DataWave**

Principal investigator: **Claudia Stephan**

Report period: **2023-11-01 to 2024-10-31**

Maximum of 15 pages including figures. 9 pt minimum font size.

Project overview

'MOD: DataWave' is an umbrella project for various sub-projects that are carried out in the department 'Modelling of Atmospheric Processes' at the Leibniz Institute of Atmospheric Physics (IAP). The resources are currently shared between six externally funded projects, which are described in the compute time proposal. They are

Since 2024:

- **DataWave** (funded by Schmidt Futures; 1 Postdoc)
- **IMPAGT** (funded by the Leibniz Association; 2 PhD, 1 Postdoc, 1 W2 position)
- **TRR181** (funded by DFG; 1 PhD, 1 Postdoc)

Since 2025:

- **ESA SciReC** (80.000 EUR for staff time)
- **Air-MOPSY** (funded by EU; 1 Postdoc)
- **SCOSTEP** visiting program: 3 months visiting PhD

With three senior scientists and two scientific programmers, a total of 14 department members are working with the ICON model on Levante. However, project 1233 has about 50 members, as we are collaborating with multiple in-house, national and international partners. The following report contains some results from last year.

Report

Since the official report period is 2023-11-01 to 2024-10-31, I cover what we achieved since 2023-11-01, but I also include more recent activities that used up nearly all resources which we were granted.

1) Review paper on gravity wave parameterizations

We published a review paper on the topic of 'Atmospheric Gravity Waves: Processes and Parameterization' [1]. We discuss how atmospheric predictability from sub-seasonal to seasonal time scales and climate variability are both influenced critically by gravity waves. The quality of regional and global numerical models relies on thorough understanding of gravity wave dynamics and its interplay with chemistry, precipitation, clouds, and climate across many scales. For the foreseeable future, gravity waves and many other relevant processes will remain partly unresolved, and models will continue to rely on parameterizations. Recent model intercomparison studies show that present-day gravity wave parameterizations do not accurately represent gravity wave processes. These shortcomings introduce uncertainties, among others, in predicting the effects of climate change on important modes of variability. However, the last decade has produced new data and advances in theoretical and numerical developments that promise to improve the situation. In our review, we give a survey of these developments, and discuss the present status of gravity wave parameterizations.

We conclude that two classes of gravity wave parameterization approaches might emerge eventually: highly efficient non-transient schemes with at best very simple descriptions of the effects of lateral propagation will be at the one end, and transient gravity wave models with full horizontal propagation at the other (see Figure 1). The latter are more expensive than the first, but they are still considerably more efficient than global gravity wave-resolving codes. They might therefore at least be a research tool guiding the improvement of the more efficient highly

simplified schemes. It will have to be seen how much those can be formulated so that the goals of scale awareness and robustness under climate variability can be achieved. An intermediate approach might be provided by the aid of machine learning that might teach us how to better formulate single-column, steady-state schemes.

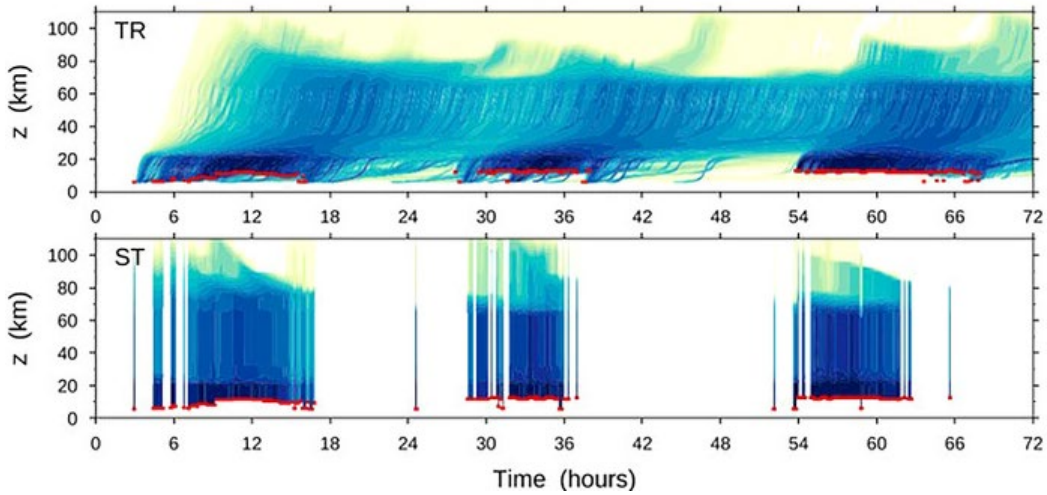

Figure 1: Westward flux from the transient MS-GWaM gravity wave parameterization coupled to ICON. There is a significant impact of gravity wave transience on the intermittency of gravity wave momentum flux. Plots show the westward gravity wave momentum flux due to convection (indicated by red) at a tropical location from a simulation either taking transience into account (TR) or assuming steady state (ST). Transience reduces the intermittency due to the variability of the source. From [1].

2) Infrasound study

We analyzed global high-resolution ICON simulations to understand the impact of stratospheric gravity waves on infrasound transmission losses across the International Monitoring System [2]. The international monitoring system (IMS, Figure 2) has been put in place to monitor compliance with the comprehensive nuclear-test-ban treaty (CTBT). Its infrasound component, dedicated to the monitoring of atmospheric events, gives also room to civil applications (e.g. monitoring of volcanic eruptions, meteorites, severe weather). Infrasound detection capabilities are largely determined by the state of the middle atmosphere. This requires an accurate knowledge of the atmospheric processes at play. Using high-resolution simulation outputs over winter 2020 (Jan 20 to March 1) we present a method to assess the impact of gravity waves on infrasound surface transmission losses across the IMS. We validate the method by comparing simulated gravity wave perturbations to lidar observations at Observatoire de Haute-Provence in France, and satellite-based gravity wave energy estimations globally. We perform propagation simulations using atmospheric specifications where gravity waves are filtered out and kept in, respectively. We demonstrate that the largest impact of gravity waves across the IMS is not where gravity wave activity is the largest, but rather where gravity wave activity combines with infrasound waveguides not firmly set in a given direction. In northern winter, the largest variations of transmission losses at 1 Hz due to gravity waves occur in the southern (summer) hemisphere in the direction of the main guide (westward propagation), with average values ranging between 10 and 25 dB in the first shadow zone. It corresponds to an average signal amplification of at least a factor 5 to 15, while this amplification is around 2 to 5 for the main guide in the northern winter hemisphere (eastward propagation).

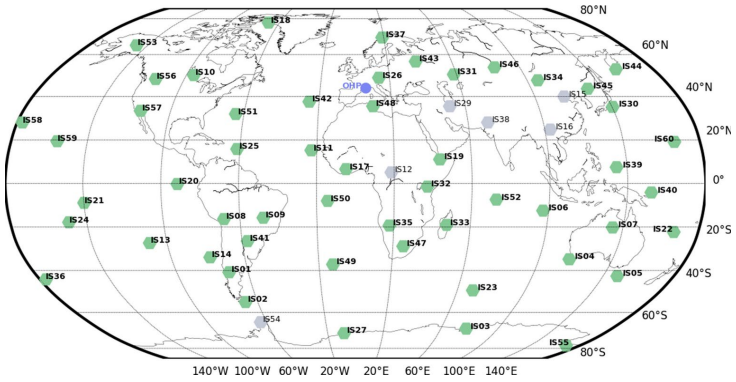

Figure 2: The infrasound component of the international monitoring system (IMS) with operational stations shown in green and planned stations in grey, as of today. The Observatoire de Haute-Provence (OHP) where lidar temperature observations are compared to ICON is marked with a blue filled circle. From [2].

3) Atmospheric energy budget

The atmospheric horizontal kinetic energy (HKE) spectrum follows a $k^{-5/3}$ power law at mesoscales (scales < 600 km). The dynamics underlying the observed mesoscale spectrum remain controversial. The prevailing explanations include a downscale cascade mediated by weakly interacting inertia-gravity waves (IGWs), strongly stratified turbulence, or interactions between waves and the balanced geostrophic flow. Our study investigates the mesoscale spectral energy budgets from storm-resolving simulations of two general circulation models, ICON and IFS [3]. The mesoscale energy fluxes within the upper troposphere and the lower stratosphere reveal different dynamics regarding the contributions from local forcing and spectral transfers (Figure 3). The stratosphere is mainly energized by upward propagating IGWs through the convergence of vertical pressure and momentum fluxes. The stratosphere also exhibits an upscale cascade mediated by nonlinear interactions between rotational modes; however, it is small compared to the energy deposited by IGWs. In contrast, the primary contribution to the mesoscale energy spectrum in the troposphere is from nonlinear spectral transfers towards small scales. Furthermore, the decomposition of the spectral transfers into the contributions from Rossby waves and IGWs reveals that their interactions dominate the downscale energy cascade. This result aligns with the hypothesis that explains the downscale cascade based on triad interactions involving vortical and gravity-wave modes. Moreover, our results suggest that weakly interacting IGWs do not contribute to the resolved kinetic energy transfers.

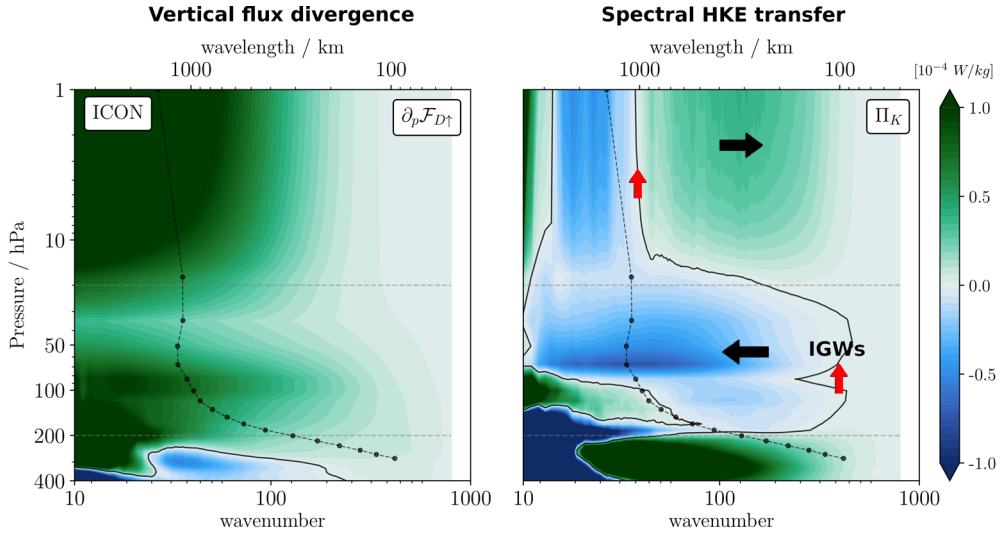

Figure 3: Cumulative energy fluxes as a function of spherical wavenumber and pressure for UA-ICON. (a) Vertical flux divergence of divergent kinetic energy (DKE), and (b) the spectral transfer of horizontal kinetic energy (HKE). The solid dotted line corresponds to the crossing scale, i.e., gravity waves dominate the HKE spectrum for wavenumbers larger than this scale.

4) Sensitivity to vertical resolution

A limitation of traditional GCMs is that the upper lid is usually located within the mesosphere (e.g., 75 km in ICON). In the upper levels, artificial damping mechanisms are introduced to prevent numerical instabilities. Additionally, the vertical resolution substantially decreases with altitude. For example, the vertical resolution in our simulations is about one kilometer near the lower stratosphere. To evaluate the impact of low vertical resolution on spectral energy transfer at mesoscales, we performed a sensitivity experiment using UA-ICON. The experiments vary the number of model levels and the vertical resolution in the stratosphere. The model lid is placed at 150 km, therefore resolving the dynamics of the stratosphere, though limited by horizontal resolution. These simulations are global, with a 20 km horizontal resolution, and were initialized on March 6, 2023. The simulations are labelled as follows: NL180, with 180 vertical levels and a nearly uniform resolution of 700 m in the stratosphere; NL90, with 90 levels and a coarser resolution of 2000 m; and NL48, with 48 levels, which also has a 2000 m resolution but in addition reduced resolution in the troposphere.

Figure 4 shows the cumulative spectral transfer of HKE for the three simulations. Below 200 hPa the results are similar across all simulations, exhibiting the expected downscale energy cascade. However, notable differences arise in the stratosphere. NL180 features a pronounced upscale transfer. The upscale transfer is weaker in NL90, with approximately half the magnitude at 50 hPa. In contrast, NL48, which also has coarser resolution in the upper troposphere, exhibits a prominent downscale cascade across most wavenumbers in the stratosphere. These results indicate that low vertical resolution affects the dynamic conditions required to capture the upscale transfer in the stratosphere and impacts the gravity wave source level, weakening the small-scale energy input necessary to sustain the upscale transfer. These results support our hypothesis that the upscale cascade in our simulations is maintained by energy injection from IGWs, which are more accurately resolved in higher-resolution simulations.

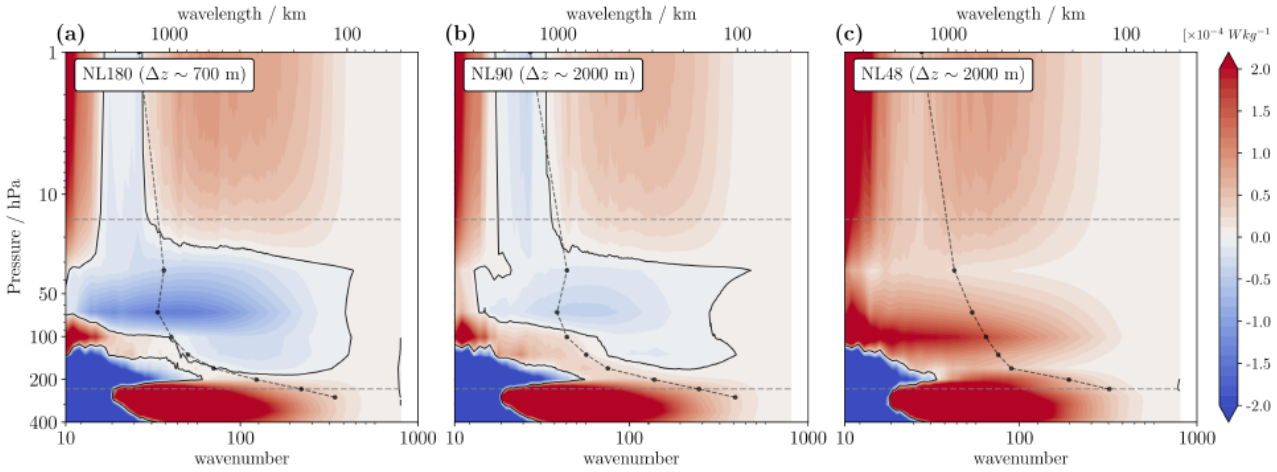

Figure 4: Cumulative spectral energy transfer as a function of spherical wavenumber and pressure for the upper-atmospheric ICON simulations with vertical level distributions in the stratosphere. NL180 with 180 levels, Δz = 700 m; NL90: 90 levels, Δz = 2000 m; NL48: 48 levels, Δz = 2000 m. Horizontal dotted lines represent pressure levels 233 and 15 hPa. The solid dotted line corresponds to the crossing scale where rotational and divergent energies intersect.

5) Resolved versus parameterized waves

We compare the parameterization schemes that represent gravity waves in the atmospheric component of the IPSLCM6 climate model and the high-resolution ICON model (Figure 5) [4]. The parameterization is run offline using ICON fields coarse-grained to a grid with a horizontal scale representative of a climate model (≈ 100 km). We then compare the parameterized gravity wave momentum fluxes and drag with those associated with the ICON fields that have been filtered out during the coarse-graining. The comparison reveals that the sum of the parameterized momentum fluxes due to mountains, convection and fronts align reasonably well with the

momentum flux from ICON in the lower stratosphere, each scheme consistently playing a dominant role where it should (frontal waves in the storm tracks, convective waves in the tropics, and mountain waves over orography). This permits physical interpretations of the origin of the gravity waves predicted by ICON, and assesses if ICON predicts about the right amount of gravity waves needed to produce a realistic middle atmosphere climate. The comparison also shows that the zonal mean gravity wave drags are also comparable but questions some of the parameter choices made when tuning the parameterizations. Analyzing the momentum flux entering in the lower stratosphere, it seems that the parameterizations overstate the contribution of the frontal waves and understate the mountain waves. Analysis of ICON momentum fluxes in the lower stratosphere also reveals an attenuation aloft the subtropical jet that is underestimated by the parameterization. Such a dynamical filtering should be corrected by tuning the characteristic phase speed or the breaking criteria of the parameterized GWs.

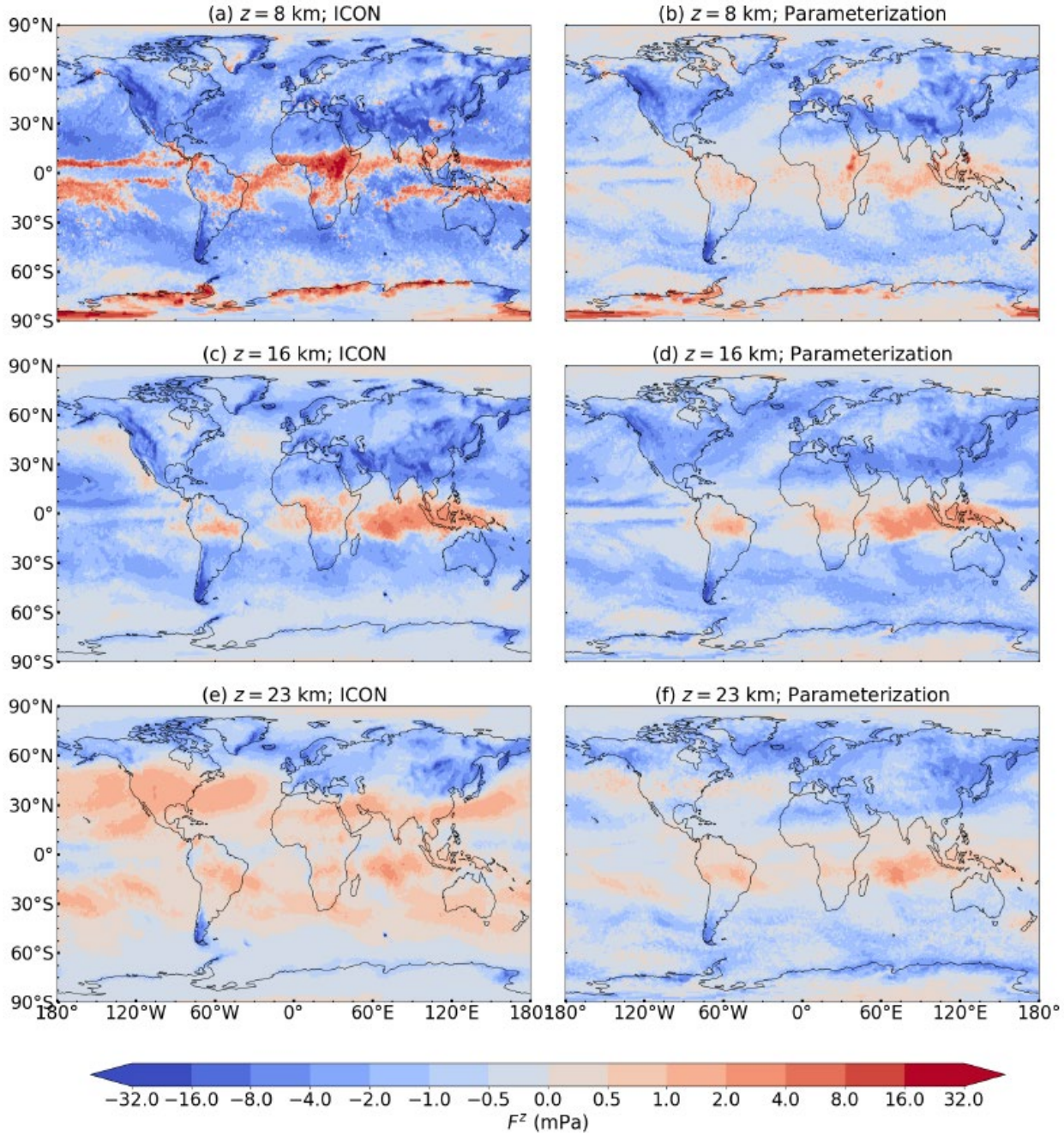

Figure 5: Global distribution of the 21-day mean net zonal momentum fluxes simulated by ICON (left) and predicted by the parameterization schemes using ICON meteorological fields (right) at (a,b) z = 8 km, (c,d) z = 16.4 km, and (e,f) z = 22.9 km. From [4].

6) Global upper-atmosphere ICON

The ICON general circulation model with upper atmosphere extension (UAICON) in the configuration with the physics package for numerical weather prediction (NWP) is presented with optimized parameter settings for the non-orographic and orographic gravity wave drag parameterizations (GWD) [5]. UAICON has been developed and applied originally using a physics package inherited from the ECHAM model, while the NWP physics have been technically implemented, but not well tuned for the mesosphere/lower thermosphere (MLT) region. In this paper, we present version uaicon-2.1 in which we implemented optimized parameter settings for the GWD parameterizations to achieve reasonable MLT temperatures and zonal winds (see Figures 6 and 7). The climatology and variability of the Northern Hemispheric stratospheric winter circulation widely improve when applying UAICON with the NWP physics package, compared to version ua-icon-1.0 with ECHAM physics. For UAICON(NWP), a statistical evaluation reveals a slight improvement in the stratosphere/mesosphere coupling, compared to version ua-icon-1.0. The GWD parameter optimization further leads to an improvement in the frequency of major sudden stratospheric warmings (SSWs). However, the seasonal distribution needs improvement and the relative frequency of split vortex SSWs is underestimated in comparison to reanalyses, as is the zonal wavenumber 2 preconditioning of SSWs, which indicates that zonal wavenumber 2 forcing in UAICON(NWP) is underrepresented. The analysis of migrating diurnal and semidiurnal tides in temperature showed a good agreement of UAICON(NWP) with SABER-derived tides and the enhancement of the migrating semidiurnal tides during SSWs is well represented in UAICON(NWP).

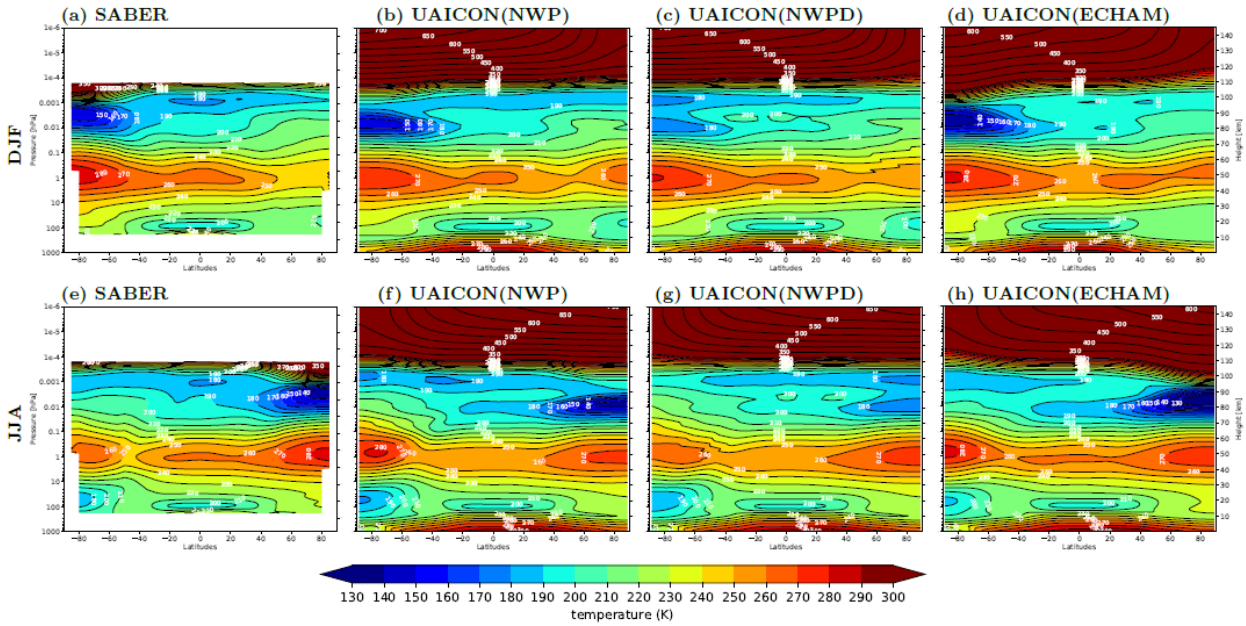

Figure 6: Climatology of zonal mean temperature for Dec./Jan./Feb. (top row a–d) and Jun./Jul./Aug. (bottom row e–h) seasonal mean; (a, e) SABER (2002–2022), (b, f) UAICON with NWP physics and tuned gravity waves; (c, g) UAICON with NWP physics (default settings); (d, h) UAICON with ECHAM physics. From [5].

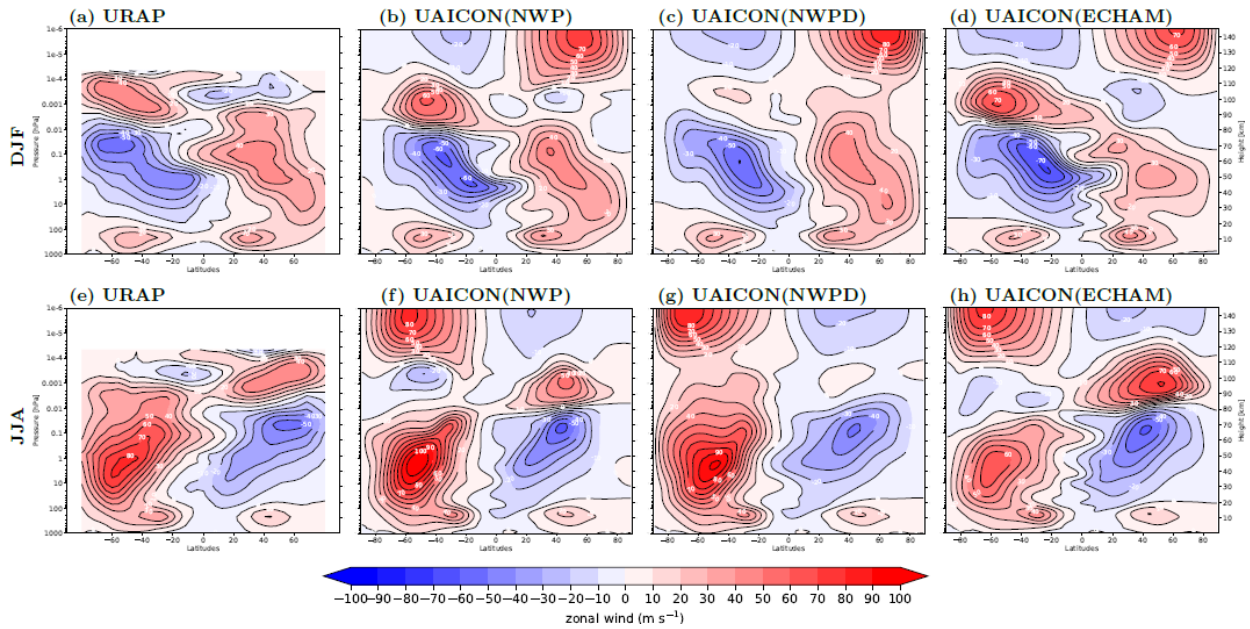

Figure 7: Climatology of zonal mean zonal wind for Dec./Jan./Feb. (top row a–d) and Jun./Jul./Aug. (bottom row e–h) seasonal mean; (a, e) URAP climatology; (b, f) UAICON with NWP physics and tuned gravity waves; (c, g) UAICON with NWP physics; (d, h) UAICON with ECHAM physics. From [5].

7) Nested UA-ICON model for the VortEx campaign

High-resolution nested simulations were conducted over Andøya, Norway (ALOMAR), to compare with mesospheric observations from the NASA 'Vorticity Experiment' (VortEx) in March 2023 (Figure 8). Observations include temperature and wind profiles up to ~80 km from the Rayleigh-Mie-Raman (RMR) lidar, as well as wind fields from the MF Saura and SIMONe radar systems. Building on the previous period's comparison (2023/2024), we also included winds from a NASA sounding rocket above ~90 km and temperature fields from the Advanced Mesospheric Temperature Mapper (AMTM). The results reported here were presented at the 2024 AGU General Assembly (Morfa et al., 2024). Figure 9 shows temperature profiles from the model, LIDAR, sounding rocket, and AMTM, averaged between 21:00–22:00 UTC. UA-ICON shows close agreement with the RMR Lidar in the stratosphere, as expected since the large scales are nudged to reanalysis. Simulations with explicitly resolved GWs show better agreement with AMTM and rocket measurements compared to the experiment with parameterized GWs (dashed line in Figure 9). Simulations with resolved GWs improve the temperature structure in the mesosphere. Overall, the simulations show reasonable agreement with observations (see also Figure 10), demonstrating UA-ICON's capability to capture key features of MLT region.

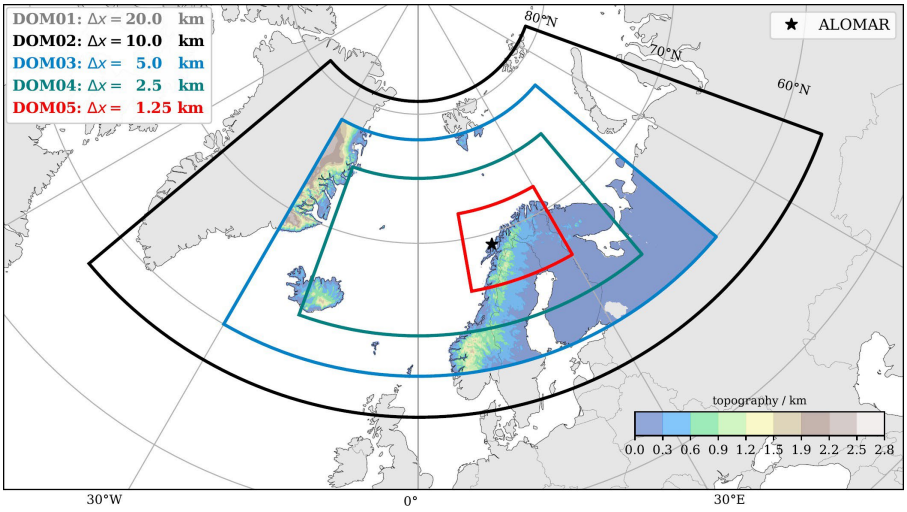

Figure 8: Experiments and domain configuration. UA-ICON was configured with 180 vertical

levels and the model top at 150 km, using a global grid at R2B7 (~20 km). One-way nesting was applied down to R2B11 (~1.25 km) through intermediate domains R2B8 (~10 km), R2B9 (~5 km), and R2B10 (~2.5 km). The large-scale dynamics were specified by nudging the global domain to ECMWF operational analyses up to an altitude of 50 km. Nudging was applied only to the global domain to constrain large-scale structures while allowing small-scale dynamics to evolve freely within the nested domains. To isolate the impact of explicitly resolved waves, we ran experiments progressively turning off non-orographic GW and convective parameterizations, starting from domain R2B9.

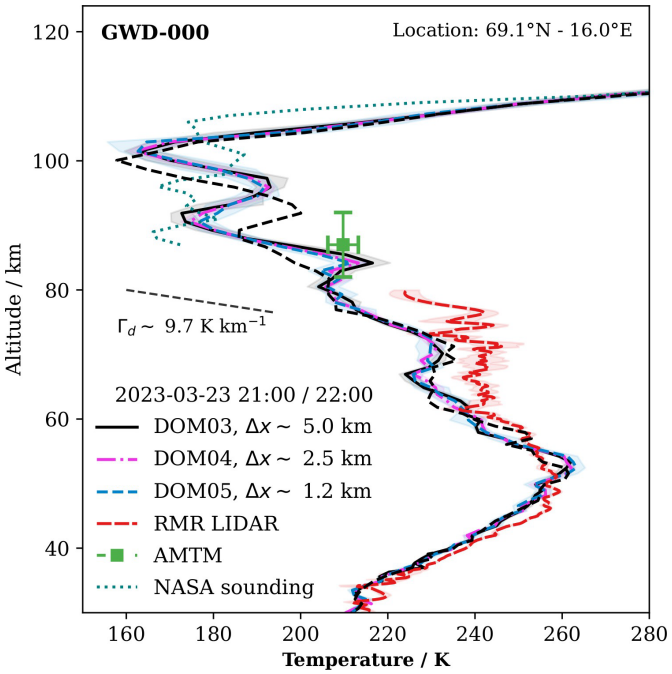

Figure 9: Simulated and observed temperature profile. The black solid line is a simulation without gravity wave drag parameterizations. The black dashed line is from a simulation that uses gravity wave drag parameterizations.

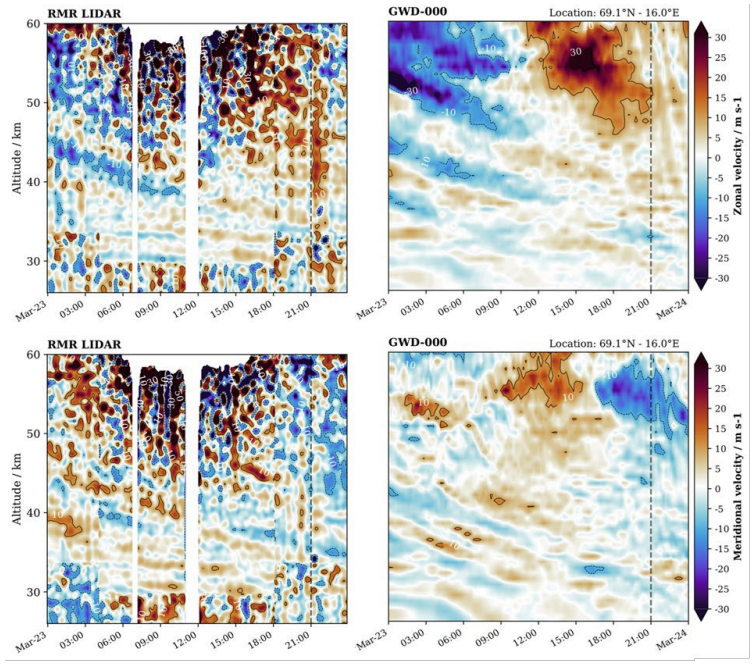

Figure 10: Simulated (right) and LIDAR-observed (left) winds.

8) Gravity waves modulated by tide DE3

We carried out a one-year long UA-ICON simulation at R2B7 resolution. We then applied the S3D method to extraxt gravity wave parameters in the thermosphere at 110 km. Figure 11 shows wave amplitude (left) and zonal background wind (right) as a funtion of longitude and month for different local times (different panels). There is a clear modulation by the nonmigrating tide DE3, which we can recognize as a zonal-wavenumber 4 pattern in both fields. This result is included in a publication on 'Challenges and gaps in understanding and monitoring low latitude F-region plasma irregularities' [6].

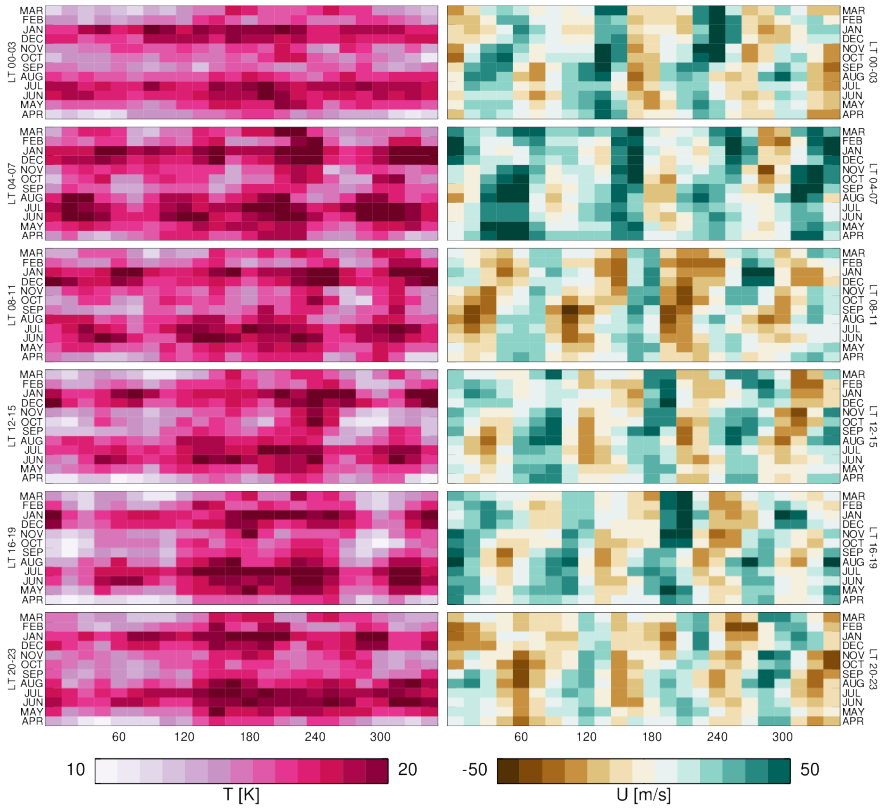

Figure 11: Local time sampling at 110 km height. Gravity waves are modulated by tide DE3.

9) Atmospheric response to sudden stratospheric warmings

We examined the time-altitude evolution of zonal wind and the time-latitude evolution of the tide SW2 in UA-ICON during the 2023 major SSW [7]. The model horizontal resolution is ~20 km (icosahedral grid R2B7) with 250 vertical levels that extend from the surface to the model top at 150 km. This corresponds to a vertical resolution of 600 m from 40–110 km. The model was nudged to the 6-hourly operational analysis of ECMWF-IFS up to a height of 50 km. The upper panel of Figure 12 shows that the model captures the occurrence of the major SSW, as expected (due to being nudged to IFS). The maximum weakening of the polar vortex occurred in the model on 17 February 2023 (one day after onset in MERRA-2), with the westward zonal mean zonal wind extending from 30 km to 75 km. The evolution of the zonal winds is in excellent agreement with MLS in the stratosphere and lower mesosphere, with subtle differences from 60–90 km (not shown). The lower panel depicts the amplitude of SW2 at 105 km. Following the polar vortex weakening, an enhancement occurred in the SW2 amplitude over mid-latitudes in both hemispheres with the maximum responses from 22–24 February 2023, 5–7 days after the maximum polar vortex weakening. The delayed response agrees with previous observations and models and may be partly explained by the time needed for the tidal wave to propagate from the lower atmosphere and establish a steady oscillation.

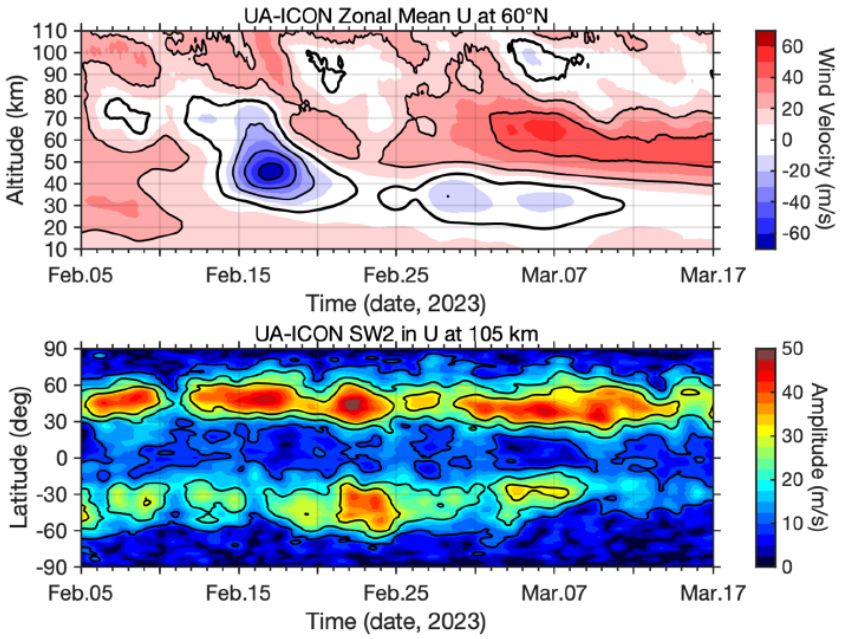

Figure 12: Results of UA-ICON simulation: (Top) Daily mean zonal mean zonal wind at 60˚N. (Bottom) Amplitude of SW2 in zonal wind at 105 km estimated using the technique of Yamazaki (2023).

10) Atmospheric response to polar vortex strength

In a second study [8] we used a 60-year free-run simulation of UA-ICON to explore the influence of stratospheric polar vortex variability on the mesosphere and lower thermosphere (MLT). The Northern Annular Mode (NAM) index and the Southern Annular Mode (SAM) index are derived from the model output to represent the strengths of the polar vortices in the Northern Hemisphere (NH) and Southern Hemisphere (SH), respectively. During weak polar vortex events in the NH, there is an increase in zonal-mean zonal winds at the NH high latitudes and a warming of the lower thermosphere, accompanied by a cooling of the mesosphere. Conversely, the wind and temperature anomalies are reversed during strong NH polar vortex events. During weak polar vortex events in the SH, similar but generally weaker anomalies are observed in the corresponding hemisphere. This study also elucidates the response of the solar-migrating semidiurnal tide (SW2) to variations in the strength of polar vortices. A weak NH polar vortex is associated with an increase in SW2, while a strong NH vortex results in a decrease in SW2. The response of SW2 to changes in the SH polar vortex is similar, although considerably weaker. The NH polar vortex variability can explain around 40−50% of the variability in the SW2 during NH winter. The SH polar vortex, however, accounts for only a small fraction of the variability (up to ~5%) in SW2.

11) Review paper on high-resolution whole-atmosphere modelling

We submitted a review paper [9] that heavily draws on UA-ICON simulations and dicusses the challenges and perspectives of modelling the whole atmosphere at fine resolution. Physics-based numerical models are essential for advancing the field of solar-terrestrial physics. Numerical models designed for terrestrial weather and climate applications usually have their model lids in the lower mesosphere. Whole-atmosphere models also cover parts of the thermosphere and ionosphere. Forecasts in this region are not nearly as accurate as those of terrestrial weather and climate. This can be attributed to a lack of observations and to the complicated structure of this region in terms of composition, thermal balance, and all aspects of multi-scale vertical coupling, transport and chemistry. Whole-atmosphere models with horizontal resolutions of several hundreds of kilometers have successfully reproduced large-scale coupling processes between the lower and upper atmosphere. With empirical prescribed forcing at the top, they can also capture the global response to geomagnetic storms and solar variability. However, it has become clear that the range of spatial scales that influence the upper atmosphere, both from above and

from below, extends to much finer scales and that resolving them requires high-resolution whole-atmosphere models. We show examples of processes that occur on regional scales (hundreds to thousands of km in the horizontal plane) and mesoscales (tens to hundreds of km). At the same time, modeling efforts need to navigate the space of physical complexity, resolution, and ensemble size, while also taking optimum advantage of available observations. In this context, we discuss advantages and disadvantages of common modeling capabilities, such as regional refinement, nudging, and data assimilation.

12) Falcon 9 re-entry

Our colleagues in the LIDAR department observed Lithium from the Falcon-9 re-entry. We performed simulation runs on R2B7 with nudging to ECMWF operational analyses initialized on 2025-02-01 at 00:00, which gives about 20 days spin-up. Trajectories are calculated by solving a Lagrangian advection problem dx ~ v* dt with 4th-order Runge-Kutta in spherical coordinates. To account for some uncertainty, we ran an ensemble of 1000 trajectories where winds are multiplied by a log-normally distributed noise with standard deviation estimated from RADAR measurements (Figure 13).

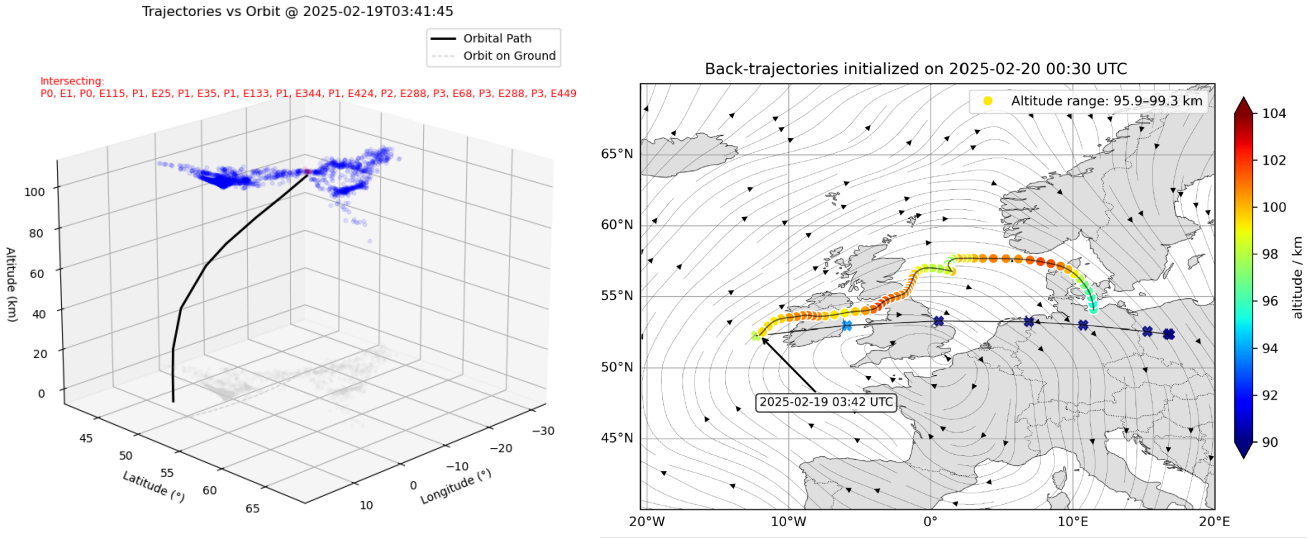

Figure 13: Trajectories starting on 2025-02-20 at 00:30:00 UTC and at an altitude of 95.9 km over Kühlungsborn (11.46 deg E, 54.07 deg N) are traced backward in time for 20 hours and 47 minutes. The mean wind for the duration of the trajectories is plotted with streamlines. The right is a 3d rendering. The ESA trajectory is shown with lines. Stars in the right mark the altitude (same colorbar).

13) Density variability

In a recent study [10] we compare radar measurements with a UA-ICON simulation. Observations of neutral density in the mesosphere lower thermosphere (MLT) region of the terrestrial atmosphere are important for understanding lower atmospheric, geomagnetic, and anthropogenic forcing. This study introduces a statistical method for observing neutral density using meteor head echoes that can be continuously observed using MST radars. The method relies on observing the mean geocentric velocity of meteor head echoes as a function of initial detection altitude and time of year. The method is demonstrated with a meteor head echo catalog, produced with the MAARSY radar in Northern Norway, which contains 1.4 million meteor head echoes between 2016–2023. Neutral density variations are observed with a 3-day time resolution and 2 km altitude resolution between 85–115 km. The measurements show variations in neutral density potentially due to geomagnetic and atmospheric events. Variations of 20–40% are common in the dataset, and agree with the magnitude of atmospheric neutral density fluctuations from a UA-ICON atmosphere model run (Figure 14). This work provides a novel method and dataset for monitoring the neutral atmospheric species in the difficult to measure MLT region.

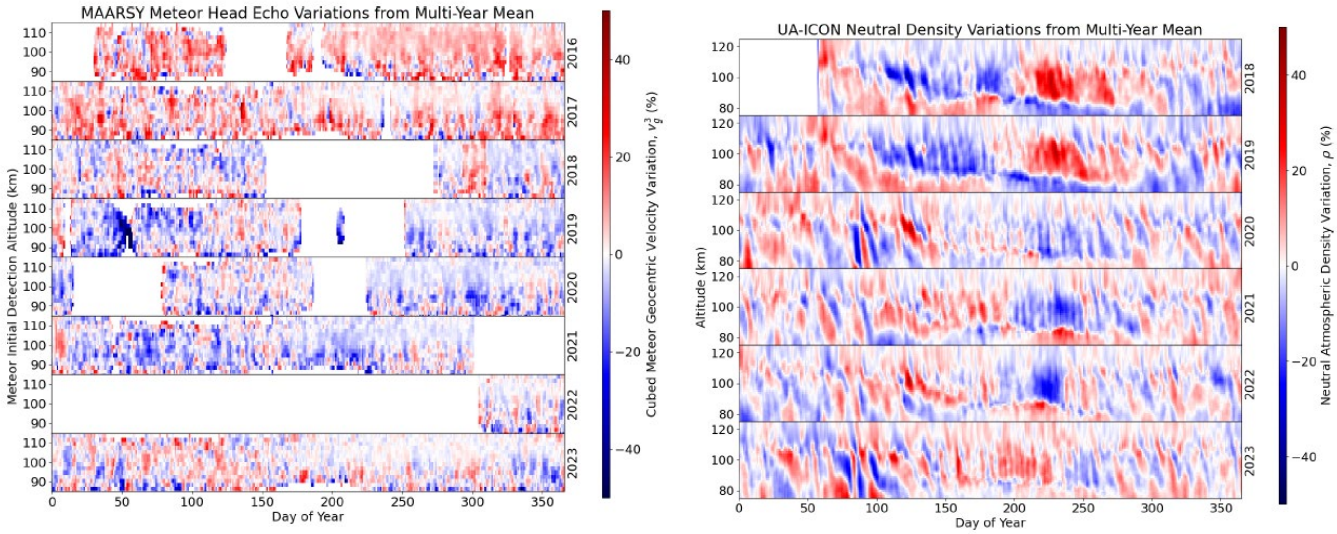

Figure 14: Left: The variation between the cubed meteor geocentric velocity for a given initial altitude detection bin with a 3-day moving mean and the cubed average of the meteor geocentric velocity for the same centered day-of-year across all measurement years. The results are presented in this manner to approximately correspond to the neutral atmospheric density for a constant ablation rate. Only data with greater than 20 meteor head echoes detected in the altitude-DOY bin are shown. Right: A free UA-ICON run for MLT neutral atmospheric density comparisons with the meteor head echo data. An analysis similar to that of the meteor head echo data was performed, where a background average was determined across the model run years and used as a baseline. In this data a 7-day multi-year running mean around the day-of-year was taken for the background model and the analyzed data was filtered with a 3-day running mean, the same as that for the meteor head echo data.

References

Members of **1233** in bold.

[1] Achatz, U., **M.J. Alexander**, E. Becker, H.-Y. Chun, A. Dörnbrack, **L. Holt**, R. Plougonven, **I. Polichtchouk**, K. Sato, A. Sheshadri, **C.C. Stephan**, A. van Niekerk and **C. Wright** (2024): Atmospheric Gravity Waves: Processes and Parameterization, 81, 237–262, J. Atmos. Sci., doi: 10.1175/JAS-D-23-0210.1

[2] C. Listowski, **C.C. Stephan**, A. Le Pichon, A. Hauchecorne, Y.-H. Kim, U. Achatz, and G. Bölöni (2024): Stratospheric gravity waves impact on infrasound transmission losses across the International Monitoring System, Pure and Applied Geophysics, doi: doi.org/10.1007/s00024-024-03467-3

[3] **Morfa Avalos, Y.A.** and **C.C. Stephan**: Mesoscale Spectral Energy Transfers in Global Storm-resolving Simulations, J. Atmos. Sci, under review

[4] I. Toghraei, F. Lott, **L. Köhler**, **C.C. Stephan** and **J. Alexander**: Can parameterizations reproduce the gravity waves momentum fluxes and drag simulated by a global high resolution model?, Geophys. Res. Lett., under review

[5] **Kunze, M., Zülicke, C.**, Siddiqui, T. A., **Stephan, C. C., Yamazaki, Y.**, Stolle, C., Borchert, S., and Schmidt, H.: UA-ICON with NWP physics package (version: ua-icon-2.1): mean state and variability of the middle atmosphere, Geosci. Model Dev. Discuss. [preprint], https://doi.org/10.5194/gmd-2024-191, accepted, 2024.

[6] Astrid Maute; Tibor Durgonics; Joseph D. Huba; Rayan Imam; Han-Li Liu; Garima Malhotra; John Retterer; **Claudia C. Stephan**; Claudia Stolle; Endawoke Yizengaw: Challenges and gaps

in understanding and monitoring low latitude F-region plasma irregularities; Surveys in Geophysics, under review

[7] V Lynn Harvey; Deepali Aggarwal; Erich Becker; Michael Bittner; Bernd Funke; Larisa Goncharenko; Jia Jia; Ruth Lieberman; Hanli Liu; Ville Maliniemi; Aurelie Marchaudon; Hilde Nesse; Noora Partamies; Nicholas Pedatella; Carsten Schmidt; Guochun Shi; **Claudia Stephan**; Gunter Stober; Willem van Caspel; Sabine Wust; **Yosuke Yamazaki**: Signatures of Polar Vortex Weakening in the MLTI: A Review, Surveys in Geophysics, under review

[8] **Akash Kumar**, Claudia Stolle, **Yosuke Yamazaki**, Nicholas M. Pedatella, **Markus Kunze**, **Claudia C. Stephan**, Tarique A. Siddiqui, MV Sunil Krishna: Impact of weak and strong stratospheric polar vortices in the northern and southern hemispheres on solar-migrating semidiurnal tides in UA-ICON, Journal of Geophysical Research: Atmospheres, under review

[9] **Claudia C. Stephan**, Han-Li Liu, Huixin Liu, Xian Lu, Astrid Maute, Nicholas M. Pedatella, Valery A. Yudin: Perspectives and Challenges in High-Resolution Whole-Atmosphere Modeling, Surveys in Geophysics, under review

[10] Devin R. Huyghebaert, Juha Vierinen, Björn Gustavsson, Ralph Latteck, Toralf Renkwitz, Marius Zecha, **Claudia C. Stephan**, J. F. Conte, Daniel Kastinen, Johan Kero, Jorge L.Chau: Long-Term Monitoring of Lower Thermospheric Neutral Density Using Meteor Head Echoes, Geophysical Research Letters, under review